Ocean Dynamics (2014) 64:1153–1161
DOI 10.1007/s10236-014-0743-4

Atmospheric boundary layer over steep surface waves

Yuliya Troitskaya · Daniil A. Sergeev · Oleg Druzhinin · Alexander A. Kandaurov · Olga S. Ermakova · Ekaterina V. Ezhova · Igor Esau · Sergej Zilitinkevich

Received: 15 October 2013 / Accepted: 25 June 2014 / Published online: 27 July 2014

Abstract Turbulent air-sea interactions coupled with the surface wave dynamics remain a challenging problem. The needs to include this kind of interaction into the coupled environmental, weather and climate models motivate the development of a simplified approximation of the complex and strongly nonlinear interaction processes. This study proposes a quasi-linear model of wind-wave coupling. It formulates the approach and derives the model equations. The model is verified through a set of laboratory (direct measurements of an airflow by the particle image velocimetry (PIV) technique) and numerical (a direct numerical simulation (DNS) technique) experiments. The experiments support the central model assumption that the flow velocity field averaged over an ensemble of turbulent fluctuations is smooth and does not demonstrate flow separation from the crests of the waves. The proposed quasi-linear model correctly recovers the measured characteristics of the turbulent boundary layer over the waved water surface.

Keywords Air-sea interaction · Quasi-linear wave model · Laboratory experiments with waves at strong winds

Responsible Editor: Huijie Xue

This article is part of the Topical Collection on the *5th International Workshop on Modelling the Ocean (IWMO) in Bergen, Norway 17-20 June 2013*

Y. Troitskaya (✉) · D. A. Sergeev · O. Druzhinin · A. A. Kandaurov · O. S. Ermakova · E. V. Ezhova
Institute of Applied Physics, Nizhny Novgorod, Russia
e-mail: yuliyatrinity@mail.ru

Y. Troitskaya · D. A. Sergeev · O. Druzhinin · A. A. Kandaurov · O. S. Ermakova · E. V. Ezhova · S. Zilitinkevich
Lobachevsky Nizhny Novgorod State University, Nizhny Novgorod, Russia

I. Esau · S. Zilitinkevich
Nansen Environmental and Remote Sensing Center, Bergen, Norway

S. Zilitinkevich
Finnish Meteorological Institute, Helsinki, Finland

S. Zilitinkevich
Division of Atmospheric Sciences and Geophysics, University of Helsinki, Helsinki, Finland

1 Introduction

The turbulent exchange processes in the ocean, in the atmosphere and across their interface have a significant impact on the earth's climate system. However, these small-scale dynamical processes are not resolved in the state-of-the-art weather and climate models but parameterized through bulk formula for aerodynamic resistance and heat exchange at the air-sea interface. Arguably, an essential part of the parameterizations is the description of the surface wave impact on the turbulent exchange.

It has been recognized that the air-sea exchange of momentum, heat and mass is mainly determined by the high-frequency part of the wave energy spectra. For instance, Caudal (1993) and Makin et al. (1995) found that about 70–80 % of surface wind stress is induced by waves with wave numbers $k>9k_p$ where k_p is a wave number corresponding to the energy peak in the surface wave spectra. About 80 % of surface roughness is determined by waves with the wavelength less than 3 m. These findings were recently corroborated by Hwang and Wang (2004), Hwang (2005), Troitskaya and Rybushkina (2008) and Troitskaya et al. (2013). Numerous instrumental and visual observations show that these short waves are steep and hence, surface wind stress is determined by extremely complicated nonlinear phenomena (e.g. sheltering and flow separation) in turbulent airflow over steep elements of the surface roughness. These phenomena were investigated by means of contact methods and smoke

visualization in laboratory experiments (Banner and Melville 1976; Kawamura and Toba 1988; Kawai 1981, 1982; Hsu and Hsu 1983; Hsu et al. 1981). Major difficulties in these experiments are related to measuring of airflow close to the water surface, especially in troughs of the waves. These measurements can be performed by a wave-following contact technique (Hsu and Hsu 1983; Hsu et al. 1981; Donelan et al. 2005). Measurements of airflow below crests of the waves can be performed by seeding the flow with small particles visualized with a strobe source of light and application of special photograph technique (Kawai 1981, 1982). Kawai's experiments demonstrated occurrence of the airflow separation from the crests of steep waves in a set of instant images.

Recently, the structure of airflow over waves has been re-investigated by a particle image velocimetry (PIV) method (Adrian 1991). In this method, the flow is seeded with small particles illuminated by laser beam, which makes them visible on digital images. Applications of the PIV by Reul et al. (1999, 2008) and Veron et al. (2007) clearly demonstrated the effect of the airflow separation from the crests of the waves and reattachment at the windward face of the wave on the instantaneous patterns of the vector velocity fields.

This paper proposes a simplified description of the revealed interaction processes coupled with the surface waves. The aim of this paper is to show that the quasi-linear approximation similar to the approach developed by Janssen (1991), Jenkins (1992), Reutov and Troitskaya (1995) and Troitskaya and Rybushkina (2008) is plausible for description of wind-wave coupling. This approach is already used in wind wave forecasting (see, e.g. Janssen 2004 and references therein). The structure of the paper is as follows. Section 2 presents the mathematical formulation of the proposed approximation model (parameterization). Section 3 describes verification of the model in physical and numerical experiments. Section 4 demonstrates an application of this model to the case of extremely high wind over the water surface. Finally, Section 5 summarizes the results.

2 Mathematical formulation of the theoretical model of turbulent wind over waved water surface

Visualization of the airflow over a steep wind waves (Troitskaya et al. 2011) clearly demonstrated that turbulent vortices are much faster than waves. Then, a model based on RANS (Reynolds-Averaged Navier–Stokes) equations can be used to describe the turbulent airflow over waves. The model readswhere the turbulence stress tensor is

$$\frac{\partial\langle u_i\rangle}{\partial t}+\langle u_j\rangle\frac{\partial\langle u_i\rangle}{\partial x_j}+\frac{1}{\rho_a}\frac{\partial\langle p\rangle}{\partial x_i}=\frac{\partial\sigma_{ij}}{\partial x_j} \tag{1}$$

$$\sigma_{ij}=\left\langle u_i^{'}u_j^{'}\right\rangle=\nu\left(\frac{\partial\langle u_i\rangle}{\partial x_j}+\frac{\partial\langle u_j\rangle}{\partial x_i}\right). \tag{2}$$

Here, <…> denotes the averaging operation over ensemble of turbulent fluctuations; ν is the turbulent eddy viscosity coefficient, which is a function of the distance, z, from the air-water interface. Application of the first order closure and a self-similarity function gives the following expression for the eddy viscosity coefficient in the turbulent boundary layer

$$\nu=\nu_a f\left(\frac{\eta\sqrt{\tau_{turb}}}{u_*}\right) \tag{3}$$

where ν_a is the air molecular viscosity. We used an empirical approximation for the function f obtained by Smolyakov (1973). It reads

$$\nu=\nu_a\left\{1+\kappa\frac{u_*\eta\sqrt{\tau_{turb}/u_*^2}}{\nu_a}\left[1-e^{-\frac{1}{L}\left(\frac{u_*\eta}{\nu_a}\right)^2\left(\frac{\tau_{turb}}{u_*^2}\right)}\right]\right\}. \tag{4}$$

In this expression, L is the scale of a viscous sub-layer, which depends on a flow regime. Smolyakov (1973) suggested L=22.4 for the aerodynamically smooth surface that gives the roughness height of 0.11 ν_a/u_*. We consider the air-water interface in our approximate model as an aerodynamically smooth curved surface.

The boundary conditions at the air-water interface $z=\xi(x, y, t)$ are as follows:

$$\frac{\partial\xi}{\partial t}+\langle u\rangle\frac{\partial\xi}{\partial x}+\langle v\rangle\frac{\partial\xi}{\partial y}\Big|_{z=\xi(x,y,t)}=\langle w\rangle|_{z=\xi(x,y,t)}, \tag{5}$$

$$\left\langle\vec{u}_\tau^{\,w}\right\rangle\Big|_{z=\xi(x,y,t)}=\left\langle\vec{u}_\tau^{\,a}\right\rangle\Big|_{z=\xi(x,y,t)}, \tag{6}$$

<u>, <v>, and <w> are the averaged air velocity components aligned with the x-, y- and z-axes. The random field of the water surface elevation is presented as a Fourier–Stieltjes transform

$$\zeta\left(\vec{r},t\right)=\int dA\left(\vec{k},\omega\right)e^{i\left(\vec{k}\,\vec{r}-\omega t\right)}.$$

Here, $\vec{k}=\left(k_x,k_y\right)$ is a two-dimensional wave vector; ω is the surface wave frequency. For a statistically homogeneous and stationary process, the wave number-frequency spectrum $F\left(\vec{k},\omega\right)$ can be introduced as follows

$$\left\langle dA\left(\vec{k},\omega\right)dA\left(\vec{k}_1,\omega_1\right)\right\rangle=F\left(\vec{k},\omega\right)\delta\left(\vec{k}-\vec{k}_1\right)\delta(\omega-\omega_1)\,d\vec{k}\,d\vec{k}_1 d\omega d\omega_1,$$

To avoid strong geometric nonlinearity, the transformation from Cartesian coordinates *(x, y, z)* to the wave-following curvilinear coordinates *(ζ_1, ζ_2, η)* is performed

$$\begin{aligned} x &= \zeta_1 + \int i\cos\vartheta \exp(i(k(\zeta_1\cos\vartheta + \zeta_1\sin\vartheta) - \omega t) - k\eta - i\varphi)dA, \\ y &= \zeta_2 + \int i\sin\vartheta \exp(i(k(\zeta_1\cos\vartheta + \zeta_1\sin\vartheta) - \omega t) - k\eta - i\varphi)dA, \\ z &= \eta + \int \exp(i(k(\zeta_1\cos\vartheta + \zeta_1\sin\vartheta) - \omega t) - k\eta - i\varphi)dA. \end{aligned} \tag{7}$$

Here, φ is the angle between the vector $\vec{k}$ and the *x*-axis. Then, in the linear approximation, the coordinate surface η=0 coincides with the waved water surface.

A solution of the RANS Eqs. (1, 2) is searched as a superposition of the mean wind field $\vec{U}_0(\eta)$ and disturbances induced in the airflow by waves at the water surface. Then, the velocity field can be written as

$$\left\langle \vec{u} \right\rangle = \vec{U}_0(\eta) + \int \vec{u}'(\eta) e^{i(k(\zeta_1\cos\vartheta+\zeta_2\sin\vartheta)-\omega t)-i\varphi-k\eta} k dA.$$

Following Jenkins (1992), we consider nonlinear equations using a quasi-linear model. The higher harmonics of perturbations are neglected. The main harmonic keeps the order of accuracy (*ka*); the average fields keep the order of accuracy $(ka)^2$. Hence, considering the equation for perturbations, we keep terms of order $(ka)^3$ if these are due to the average wave-induced fields and neglect them if they are due to nonlinear interaction between first and second harmonics. This approach is applicable for small Reynolds numbers (see Batchelor 1967). In the turbulent regime of the flow, the Reynolds number as defined by the molecular viscosity is huge, but the average flow dynamics described within the Reynolds equations is determined by the effective Reynolds number (e.g. Esau 2004), which is defined by the eddy viscosity coefficient. The effective Reynolds number for the wave disturbances induced in the airflow Re_{eff} was estimated by Troitskaya et al. (2011) as a value of order (*ka*) assuming that the velocity scale, u_{wave}, is of order *cka* and the viscosity coefficient is $\nu_{turb}=ku_*z$. Taking into account that the vertical scale of the turbulent boundary layer for the wave disturbances is $\delta=u_*/ck$ (Troitskaya and Rybushkina 2008), the estimation can be written as $Re_{eff}=\delta k u_{wave} z/\nu_{turb} \sim ka < 1$. Thus, the small Re_{eff} justifies the use of a linear approximation in the proposed formulation.

Let us now consider the equations for the disturbances induced by a single harmonic wave at the water surface with the wave vector $\vec{k}$, frequency ω and amplitude *dA*. We introduced a formal coordinate transformation, where the coordinate line η=0 coincides with the water surface disturbed by this single harmonic wave

$$\begin{aligned} x &= \zeta_1 + i\cos\vartheta e^{i(k(\zeta_1\cos\vartheta+\zeta_2\sin\vartheta)-\omega t)-k\eta-i\varphi} dA, \\ y &= \zeta_2 + i\sin\vartheta e^{i(k(\zeta_1\cos\vartheta+\zeta_2\sin\vartheta)-\omega t)-k\eta-i\varphi} dA, \\ z &= \eta + dA\, e^{i(k(\zeta_1\cos\vartheta+\zeta_2\sin\vartheta)-\omega t)-i\varphi-k\eta}. \end{aligned} \tag{8}$$

The linear coordinate transformation

$$\begin{aligned} \zeta'_1 &= \zeta_1\cos\vartheta + \zeta_2\sin\vartheta - \frac{\omega}{k}t, \\ \zeta'_2 &= \zeta_2\cos\vartheta - \zeta_1\sin\vartheta = y_2\cos\vartheta - y_1\sin\vartheta = y' \end{aligned} \tag{9}$$

defines the reference frame following this harmonic wave, where the wave field does not depend on ζ'_2 (or Cartesian coordinate y'), i.e. it depends only on two coordinates ζ'_1 and η. The tangential velocity components are transformed similarly to (9). They read in the new reference frame as

$$\begin{aligned} u' &= u\cos\vartheta + v\sin\vartheta - \frac{\omega}{k}, \\ v' &= -u\sin\vartheta + v\cos\vartheta. \end{aligned} \tag{10}$$

A stream function Φ can be introduced for the motions in the plane $\zeta'_2 = y' = const$ as follows

$$u' = \frac{\partial\Phi}{\partial\eta}; w = -\frac{\partial\Phi}{\partial\zeta'_2}.$$

The RANS equations can be rewritten in terms of the introduced stream function, Φ, and vorticity, χ, as

$$\begin{aligned} &\frac{\partial\chi}{\partial t} + \frac{1}{I}\frac{\partial\chi}{\partial\zeta'_1}\left(\frac{\partial\Phi}{\partial\eta}\right) - \frac{1}{I}\frac{\partial\chi}{\partial\eta}\left(\frac{\partial\Phi}{\partial\zeta'_1}\right) = \Delta(\nu\chi) - \frac{2}{I^2}\nu_{\eta\eta}\frac{\partial^2\Phi}{\partial{\zeta'_1}^2} - \\ &-\frac{I_\eta}{I^3}\left(\left(\Phi_\eta\nu_\eta\right)_\eta - \nu_\eta\Phi_{\zeta'_1\zeta'_1}\right) - \frac{I_{\zeta'_1}}{I^3}\left(2\nu_\eta\Phi_{\zeta'_1\eta} - \Phi_{\zeta'_1}\nu_{\eta\eta}\right) + \Phi_\eta\nu_\eta\frac{I_{\zeta'_1}^2 + I_\eta^2}{I^4}, \end{aligned} \tag{11a}$$

$$\Delta\Phi = \chi = \frac{1}{I}\left(\Phi_{\zeta'_1\zeta'_1} + \Phi_{\eta\eta}\right), \tag{11b}$$

where *I* is the Jacobian of transformation (8). The transversal velocity component v' does not enter the Eq. (11a, 11b). It could be found from the equation

$$\frac{\partial v'}{\partial t} + \frac{1}{I}\left(\frac{\partial v'}{\partial\zeta'_1}\frac{\partial\Phi}{\partial\eta} - \frac{\partial v'}{\partial\eta}\frac{\partial\Phi}{\partial\zeta'_1}\right) = \Delta(v'\nu) + \frac{1}{I}v'_\eta\nu_\eta. \tag{12}$$

We search the solution to the system (11a, b) and (12) as a superposition of the mean field and harmonic wave disturbance in the following form

$$\Phi = \int \left(U_0(\eta)\cos\vartheta + V_0(\eta)\sin\vartheta - \frac{\omega}{k}\right)d\eta + \Phi_1(\eta)dA\, e^{ik\zeta'_1}, \tag{13a}$$

$$v = V_0(\eta)\cos\vartheta - U_0(\eta)\sin\vartheta + V_1(\eta)dA\,e^{ik\zeta_1'}, \tag{13b}$$

$$\chi = U_{0\eta}\cos\vartheta + V_{0\eta}\sin\vartheta + X_1(\eta)dA\,e^{ik\zeta_1'}. \tag{13c}$$

The complex amplitudes, $\Phi_1(\eta)$,$\chi_1(\eta)$ and $V_1(\eta)$, are obtained from the linearization of (11a, b) and (12) as

$$(\Phi_{0\eta}X_1 - \Phi_1\chi_{0\eta})ik - \left(\frac{d^2}{d\eta^2} - k^2\right)(X_1\nu) = -2\nu_\eta\Phi_1k^2 - 2kAe^{-k\eta}\left(\Phi_{0\eta}\nu_\eta\right)_\eta, \tag{14a}$$

$$\frac{d^2\Phi_1}{d\eta^2} - k^2\Phi_1 = X_1 - 2ke^{-k\eta}\Phi_{0\eta\eta} \tag{14b}$$

and

$$\left(\Phi_{0\eta}V_1 - \Phi_1\widehat{V}_\eta\right)ik = \nu\left(\frac{d^2}{d\eta^2} - k^2\right)V_1 + \nu_\eta V_{1\eta}k^2 \tag{15}$$

We look only for bounded solutions to the system (14a, b) and (15), which are decreasing at large distances from the surface, i.e.

$$\Phi_1|_{\eta\to\infty}\to 0; \quad V_1|_{\eta\to\infty}\to 0.$$

The boundary conditions at the water surface for the system (14a, b) are obtained from (20) and (6). They are expressed in curvilinear coordinates (Reutov and Troitskaya 1995) as

$$\Phi_1|_{\eta=0} = 0; \quad \Phi_{1\eta}|_{\eta=0} = 2\omega; \quad V_1|_{\eta\to 0} = 0 \tag{16}$$

The only nonlinear effect taken into account in the quasi-linear approximation here is the demodulation of the wave disturbances induced in the airflow by waves at the water surface.

Equations for the mean velocity components $U_0(\eta)$ and $V_0(\eta)$ are obtained by the following steps. Averaging of (11a, b) over ζ'_1 gives equation for Φ_0 and averaging of (12) yields equation for $v_0(\eta)$. $U_0(\eta)$ and $V_0(\eta)$ are expressed through $\Phi_0(\eta)$ and $v_0(\eta)$ by inversion of (13a, b) and then integrated over wave numbers and frequencies, which gives

$$\frac{d}{d\eta}\left(\nu\frac{d(U_0, V_0)}{d\eta}\right) = \int\left(\tau_\parallel(\eta,k,\varphi,\omega)(\eta)\begin{pmatrix}\cos\varphi\\ \sin\varphi\end{pmatrix} + \tau_\perp(\eta,k,\varphi,\omega)(\eta)\begin{pmatrix}-\sin\varphi\\ \cos\varphi\end{pmatrix}\right)k^2F(k,\varphi,\omega)kdkd\varphi d\omega\ . \tag{17}$$

Here, $\tau_{||}(\eta, k, \theta, \omega)(\eta)$, $\tau_\perp(\eta, k, \theta, \omega)(\eta)$ are the components of the momentum flux induced by the surface waves with wave number k and frequency ω propagating at the angle θ to the wind. The expression for $\tau_{||}(\eta, k, \theta, \omega)(\eta)$ follows from (11a, b)

$$\tau_\parallel(\eta,k,\varphi,\omega)(\eta) = k\left[k\nu_\eta\mathrm{Re}\left(\Phi_{1\eta} - k\Phi_1\right)e^{-k\eta} + 2k^2e^{-2k\eta}\nu_\eta U_0\cos\varphi\right]$$

and expression for $\tau_\perp(\eta, k, \theta, \omega)(\eta)$ follows from (12)

$$\tau_\perp(\eta,k,\omega) = -\frac{1}{2}k\frac{d}{d\eta}\mathrm{Im}\left(\Phi_1^*V_1\right).$$

Equation (17) expresses the conservation law for the vertical flux of two projections of the horizontal momentum component in the turbulent boundary layer. If the turbulent shear stress at a large distance from the surface is aligned with x-axis, the conservation law for the mean momentum components may be written as

$$\tau^{(x)}_{turb}(\eta) + \tau_{||}(\eta) = u_*^2,$$
$$\tau^{(y)}_{turb}(\eta) + \tau_\perp(\eta) = u_*^2.$$

According to (17), the nonlinear addition to the wind velocity is determined by the surface wave spectrum $S(\omega, k)$, which shape is critical for the proposed model. In order to determine the empirical shape of the spectrum, laboratory experiments have been conducted where the airflow velocity profile and the elevation of the water surface in three close points were measured simultaneously. These data are sufficient to retrieve the three-dimensional $S(\omega, k)$ for calculations of the form drag and the model verification. Recently, the model has been also generalized to include cases of the stratified atmosphere over the ocean (Troitskaya et al. 2013).

3 Verification of the proposed model through laboratory and numerical experiments

The proposed quasi-linear approximation greatly simplifies the description of the wind-wave interaction. In particular, the aerodynamic roughness of the water surface in this approximation is determined only by the surface wave spectrum $S(\omega, k)$. The wind-wave interaction models beyond this approximation require information about the higher statistical moments of the surface wave field, which is not available in applications. However, the proposed approximation utilizes several strong assumptions, which need to be verified. The subsections below describe verification of this quasi-linear model through laboratory and numerical experiments.

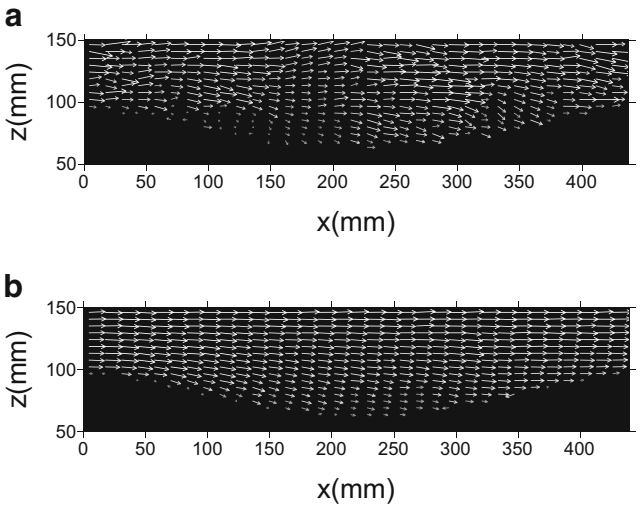

Fig. 1 The vector velocity field in the airflow over a paddle-generated wave in the wave-following reference frame. The velocity vectors were retrieved from a high-speed video filming by a digital particle image velosimetry technique. The wind friction velocity is u_*=200 mm/s, the wavelength k=0.15 cm^{-1}, and the slope ka=0.25. **a** The instantaneous pattern. **b** The ensemble averaged pattern

3.1 Laboratory experiments on airflow over steep waves

The turbulent airflow over waves was studied in a physical laboratory experiment using a video-PIV method and applications of the high-speed video photography (see Troitskaya et al. 2013). Alternatively, to the classical PIV technique, this approach generates statistical ensembles of instantaneous velocity field realizations. The experiments were performed in a round wind–wave channel at the Institute of Applied Physics, Russian Academy of Sciences. A fan generated the airflow with the centerline velocity 4 m/s. The surface waves were generated by a programmed wave-maker at the frequency of 2.5 Hz with the amplitudes of 0.65, 1.4 and 2 cm. The working area (27.4 × 10.7 cm^2) was at a distance of 3 m from the fan. To perform the measurements of the instantaneous velocity fields, spherical polyamide particles 20 μm in diameter were injected into the airflow. The images of the illuminated particles were taken with a digital CCD video camera at a rate of 1,000 frames per second. A statistical ensemble of 30 movies with duration from 200 to 600 ms was obtained for a given set of parameter characterizing the wind and wave regimes. Individual flow realizations manifested the typical features of flow separation. The average vector velocity fields obtained by the phase averaging of the individual vector fields were smooth and slightly asymmetric. The minimums of the averaged horizontal velocity near the water surface were shifted to the leeward side of the wave profile but did not indicate flow separation (compare Fig. 1a, b).

The results of these measurements were compared with the calculations within the quasi-linear model of turbulent boundary layer. The wave parameters (wavelength, celerity, steepness), used in this comparison of theory with experiment, were retrieved from the same video films as those used for the airflow velocity calculations. The model calculations were in a good agreement with the experimentally measured and conditionally averaged mean wind velocity, turbulent stress and also amplitude and phase of the main harmonics of the wave-induced velocity components (see Fig. 2a, b). The wave-induced pressure perturbations, averaged over the turbulent fluctuations, were retrieved by Troitskaya et al. (2011) from the measured velocity fields, using the Reynolds equations. It ensures sufficient accuracy for study of the dependence of the wave increment on the wave amplitude. The theoretical curves for magnitude and phase of wave-induced pressure fluctuations are in a good agreement with the experimental data (see Fig. 3b, c). The quasi-linear model also

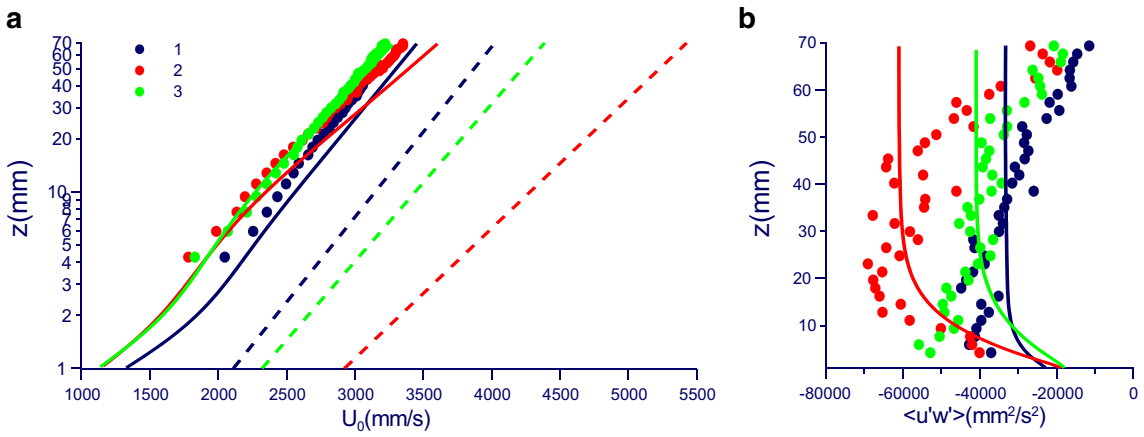

Fig. 2 Intercomparison between experiments (*coloured dots*) and the theory (lines corresponding to the concrete experiment conditions identified by the colour): **a** the mean velocity profiles and **b** the stress profiles. *Solid lines* are the calculations with the quasi-linear model for the measured parameters of the wave and the wind (see Troitskaya et al. 2011). *Dashed lines* are the calculations with the same model and parameters but for the aerodynamically smooth surface

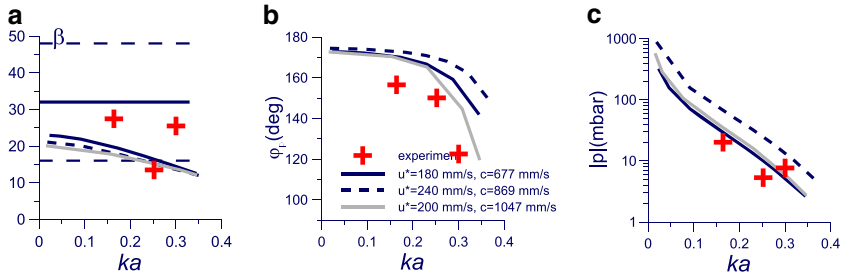

Fig. 3 Intercomparison between experiments (*crosses*) and the theory (*s*) for the dependence on the wave steepness of: **a** β, **b** the phase shift, and **c** the normalized magnitude of the first harmonic of wave-induced pressure disturbance at the water surface. *Solid dark lines* are for the model with u_* =180 mm/s, c=677 mm/s; *dashed dark lines* are for u_*=240 mm/s, c=869 mm/s; and *solid light lines* are for u_*=200 mm/s, c=1047 mm/s

reproduces the wind-wave interaction parameter as it was introduced by Miles (1957) (see Fig. 3a):

$$\beta = \frac{2}{(ka)^2 \rho u_*^2} \frac{1}{\lambda} \int_0^{\lambda} \langle p \rangle \frac{dz_b}{d\xi} d\xi.$$

3.2 Direct numerical simulations of the airflow over steep waves

Direct numerical simulations (DNSs) of the airflow over finite amplitude periodic surface wave (Druzhinin et al. 2012) have also supported the proposed approximate model. These DNSs modelled two-dimensional water waves with the wave slopes in the range ka=0–0.2 in the flow with the bulk Reynolds number Re=15,000. Different wave age parameters in the range c/u_*=0–10 where u_* is the friction velocity and c is the wave celerity were considered. The shape of the water waves was prescribed and did not evolve under the action of the wind. The numerical algorithm is similar to that in Sullivan et al. (2000) but adjusted for a staggered grid. The computational domain (periodic in the x- and y-directions) had the size $L_x=6\lambda$, $L_y=4\lambda$ and $L_z=\lambda$. The DNS code is solving fully three-dimensional Navier–Stokes equations in curvilinear coordinates in a frame of reference moving with the phase velocity of the wave. The flow is driven by the shear, which is created by the upper plane boundary moving horizontally in the x-direction with a prescribed bulk velocity. Nonslip boundary conditions applied at the top and bottom boundaries of the domain. The model mesh had 360×240×180 nodes in the x-, y-, and z-directions correspondingly. The Adams–Bashforth method is employed to advance integrations in time, and the equation for pressure is solved iteratively by using the fast Fourier transformation in x- and y-directions and the Gauss method in z-direction. The computations were carried out for 12,000 time steps, which is equal to 200 dimensionless large-scale time units (based on the bulk velocity and the wave length). Each time unit typically corresponds to about 20 viscous time units, $1/(\mathrm{Re}u_*^2)$. Ensemble-averaged velocity and pressure fields were evaluated from 500 instantaneous flow-field data samples which covered the time period of 100 large-scale time units. Profiles of the mean velocity and turbulent stresses were obtained by averaging over the wavelength.

As in the physical experiment, the instantaneous realizations of the velocity field in DNS showed the flow separation at the crests of the waves. However, the ensemble-averaged velocity fields had typical structures similar to those excising in the shear flows near critical levels, where the phase velocity of the disturbance coincides with the flow velocity (Fig. 4). Generally, DNS runs support the approximations in the proposed model when profiles of the mean wind velocity, the turbulent stress, amplitude and phase of the main harmonics of the wave-induced velocity components, wave-induced pressure fluctuations and wind wave growth rate are considered (Druzhinin et al. 2012).

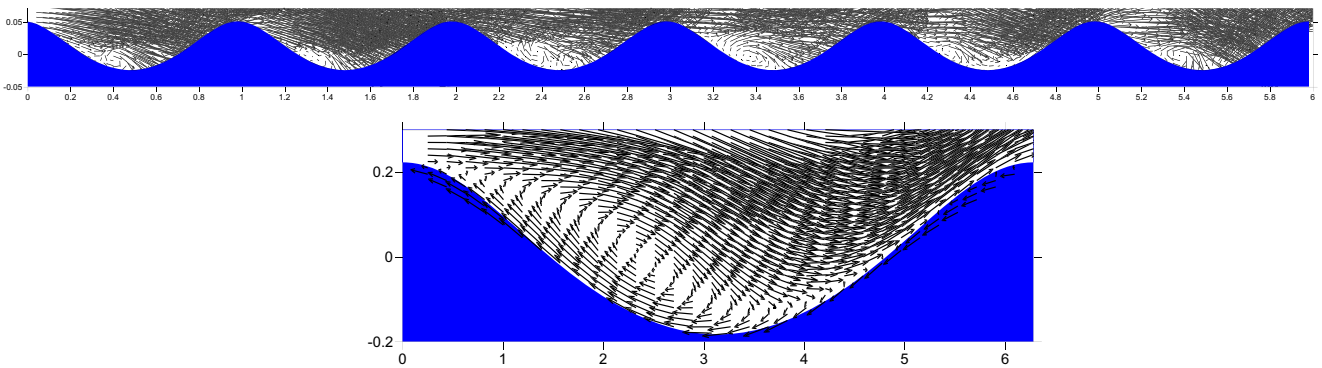

Fig. 4 A longitudinal cross-section of the instantaneous (upper panel) and average (lower panel) velocity vector fields for ka=0.2 and c=0.1

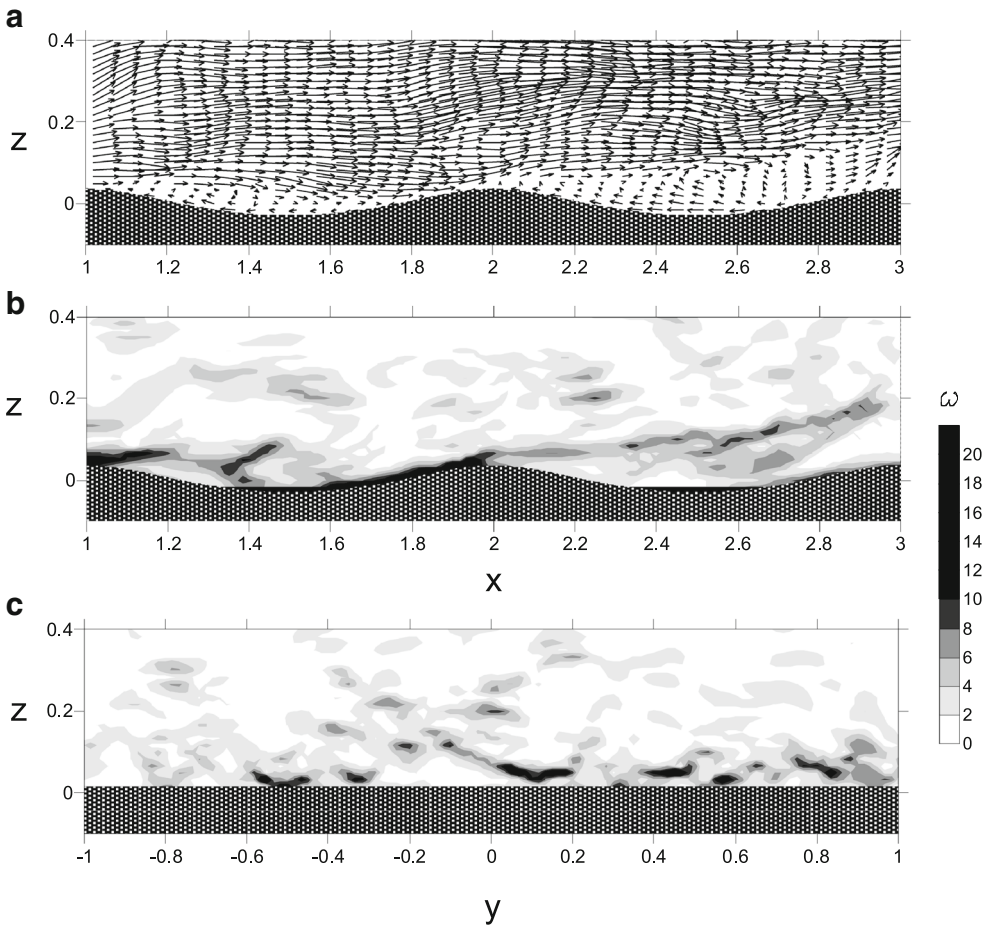

Fig. 5 A longitudinal cross-section of the instantaneous velocity (**a**) and vorticity modulus (**b**, **c**) fields obtained in DNS for ka=0.2 and c=0.1

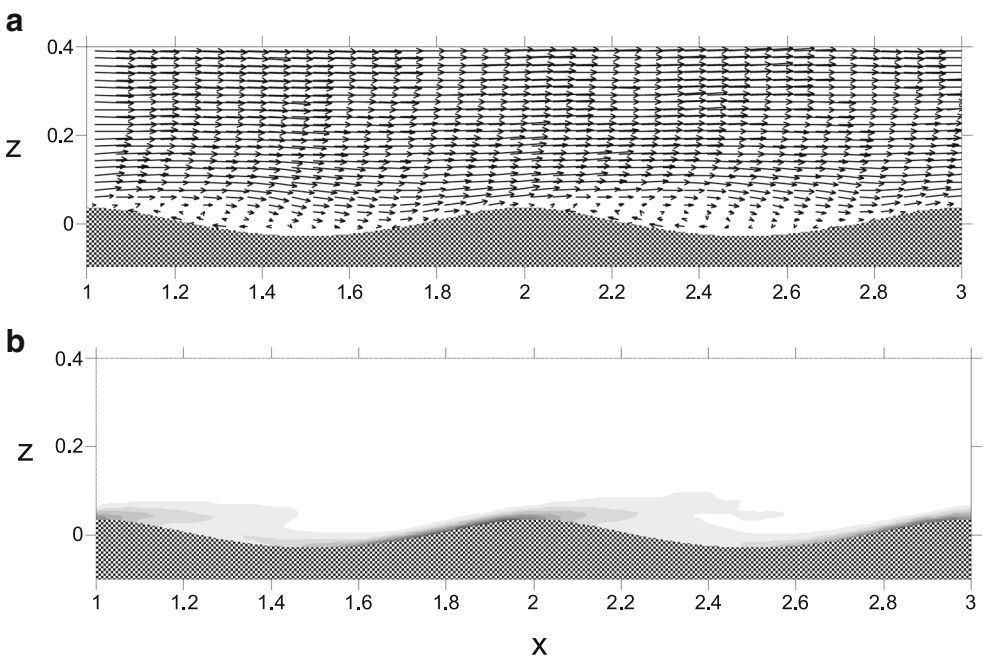

Fig. 6 The same instantaneous fields as in Fig. 5, but averaged along the wave front

Moreover, DNS results suggest that the nonseparating quasi-linear theory is applicable because of the development of strong heterogeneity of the separation zone in the transverse direction (i.e. along the wave front). Vorticity in the airflow over a steep wave appears to be concentrated in thread-like vortex structures, which have a horseshoe shape and resemble well-known λ-vortices extensively studied in the case of a "classical" boundary layer over a solid plane boundary (Moin and Kim 1985; Esau 2003; Esau et al. 2013). The instantaneous flow velocity and vorticity fields averaged *only* along the wave front (and *not* in time) are nonseparating. Figures 5 and 6 compare the distributions of the instantaneous velocity and vorticity modulus fields obtained in DNS (Fig. 5) and the same *instantaneous* fields after averaging along the front (Fig. 6). Figure 1 clearly shows a λ-vortex separating from the wave crest at x=2. Here, the instantaneous flow has a separation zone. However, the y-averaged vorticity and velocity fields are smooth, nonseparating and characterized by the well-known Kelvin's "cat eye" pattern.

4 Verification of the quasi-linear model at strong winds

Wind–wave interaction at extreme wind speed is of special interest now in connection with the problem of explanation of the sea surface drag saturation at the wind speed exceeding 30 m/s. The idea on saturation (and even reduction) of the coefficient of aerodynamic resistance of the sea surface at hurricane wind speed has been first suggested in Emanuel (1995) on the basis of theoretical analysis of the maximum wind speed sensitivity in a hurricane to the ratio of enthalpy and momentum exchange coefficients. Both the field campaigns (Powell et al. 2003; Black et al. 2007) and laboratory experiments (Donelan et al. 2004) confirmed that at the hurricane wind speeds, the sea surface drag coefficient, C_{D10}, is significantly reduced in comparison with the parameterization calibrated to moderate to strong wind conditions (Garratt 1977; Fairall et al. 2003).

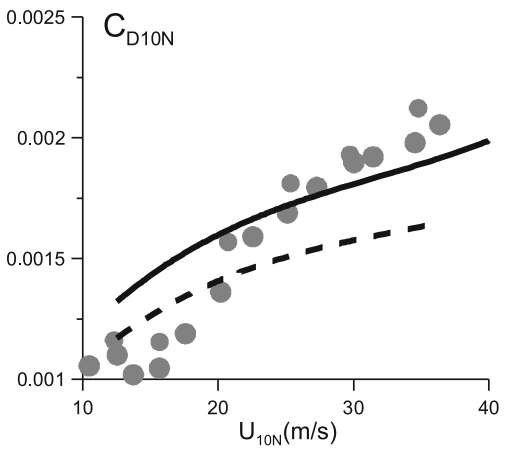

Fig. 7 The dependence of the surface drag coefficient on the wind speed. The laboratory experiments are represented by *dots*. The model calculations are represented by the *solid line* with a short wave spectrum of surface waves and by the *hatch line* without the short wave spectrum of the surface waves

We supposed that this reduction could be due to changes in the form drag of surface waves at strong wind conditions. To verify the supposition, we simultaneously measured aerodynamic resistance of the water surface and frequency-wave number spectra of the wind waves in a wide range of the wind speeds achievable in the laboratory tank of the Institute of Applied Physics (Troitskaya et al. 2013). The wind friction velocity and C_{D10} were retrieved from the measurements by the profile method. As Donelan et al. (2004), the experiments revealed changes in C_{D10} at high wind conditions but the growth rate of C_{D10} was decreasing when U_{10} exceeds 25 m/s. This is in broad agreement with Vickery et al. (2009), Holthuijsen et al. (2012) and Hwang et al. (2013) results but distinct to the results of Donelan et al. (2004) where such a decrease has been found only for U_{10}>30 m/s. The dependences from our experiments are compared with the quasi-linear model predictions for the turbulent boundary layer over the waved water surface (see Fig. 7). The quantitative agreement is found when momentum flux due to the short wave part of the wind wave spectra has been taken into account.

5 Conclusions

In this study, we introduced an approximate quasi-linear model for the description of the turbulent boundary layer over steep surface waves. This model assumes that wave-induced disturbances of the atmospheric turbulent boundary layer could be reasonably described in a linear approximation with the momentum flux from wind to waves retained as the only nonlinear effect in the model.

The model has been further verified with a set of the original laboratory and numerical experiments. The laboratory experimental study of the airflow over the steep waves was performed by means of the PIV technique. The numerical study was performed with DNS of the turbulent airflow over waved surface at Re=15,000.

Both the physical and numerical experiments supported reasonable quality of the proposed approximate model in the case of strong winds. Moreover, the model was able to take into account the effects of the anomalously low aerodynamic drag at strong winds. This effect was explained by a saturation of the form drag of the water surface.

Acknowledgments This work is supported by grant of the government of the Russian Federation (contract 11.G34.31.0048), Federal Targeted Program "Scientific and Pedagogical Staff for Innovative Russia" for 2009–2013 and by RFBR (13-05-00865, 13-05-97068, 13-05-12093) and by the bilateral Norwegian-Russian project CLIMARC. Alexander

Kandaurov and Olga Ermakova acknowledge partial support from Russian Science Foundation (Agreement No. 14-17-00667).

References

Adrian RJ (1991) Particle imaging techniques for experimental fluid mechanics. Annu Rev Fluid Mech 23:261–304

Banner ML, Melville WK (1976) On the separation of airflow over water waves. J Fluid Mech 77:825–842

Batchelor G K (1967) An introduction in fluid dynamics. Cambridge University Press. 615 pp

Black PG, D'Asaro EA, Drennan WM, French JR, Niiler PP, Sanford TB, Terrill EJ, Walsh EJ, Zhang JA (2007) Air–sea exchange in hurricanes: synthesis of observations from the coupled boundary layer air–sea transfer. Exp Bull Am Meteorol Soc 88(3):357–374

Caudal G (1993) Self-consistency between wind stress, wave spectrum, and wind-induced wave growth for fully rough air-sea interface. J Geophys Res 98(C12):22743–22752

Donelan MA, Haus BK, Reul N, Plant WJ, Stiassnie M, Graber HC, Brown OB, Saltzman ES (2004) On the limiting aerodynamic roughness of the ocean in very strong winds. Geophys Res Lett 31, L18306

Donelan MA, Babanin AV, Young IR, Banner ML, McCormick C (2005) Wave follower field measurements of the wind input spectral function. Part I: measurements and calibrations. J Atmos Oceanic Tech 22(7):799–813

Druzhinin O A, Troitskaya Y I, Zilitinkevich S S (2012) Direct numerical simulation of a turbulent wind over a wavy water surface. J Geophys Res 117(C00J05). doi:10.1029/2011JC007789

Emanuel KA (1995) Sensitivity of tropical cyclones to surface exchange coefficients and a revised steady-state model incorporating eye dynamics. J Atmos Sci 52(22):3969–3976

Esau I (2003) Coriolis effect on coherent structures in planetary boundary layers. J Turbul 017

Esau I (2004) Simulation of Ekman boundary layers by large eddy model with dynamic mixed subfilter closure. Environ Fluid Mech 4(3): 273-303

Esau I, Davy R, Outten S, Tyuryakov S, Zilitinkevich S (2013) Structuring of turbulence and its impact on basic features of Ekman boundary layers. Nonlinear Process Geophys 20:589–604

Fairall CW, Bradley EF, Hare JE, Grachev AA, Edson JB (2003) Bulk parameterization of air–sea fluxes: updates and verification for the COARE algorithm. J Climate 16(4):571–591

Garratt JR (1977) Review of drag coefficients over oceans and continents. Mon Weather Rev 105:915–929

Holthuijsen L H, Powell M D, Pietrzak J D (2012) Wind and waves in extreme hurricanes. J Geophys Res 117(C09003). doi:10.1029/2012JC007983

Hsu CT, Hsu EY (1983) On the structure of turbulent flow over a progressive water wave: theory and experiment in a transformed wave-following coordinate system. Part 2. J Fluid Mech 131:123–153

Hsu CT, Hsu EY, Street RL (1981) On the structure of turbulent flow over a progressive water wave: theory and experiment in a transformed, wave-following co-ordinate system. J Fluid Mech 105:87–117

Hwang P A (2005) Wave number spectrum and mean square slope of intermediate-scale ocean surface waves. J Geophys Res 110(C10029). doi:10.1029/2005JC003002

Hwang PA, Wang DW (2004) An empirical investigation of source term balance of small scale surface waves. Geophys Res Lett 31, L15301. doi:10.1029/2004GL020080

Hwang PA, Burrage DM, Wang DW, Wesson JC (2013) Ocean surface roughness spectrum in high wind condition for microwave backscatter and emission computations. J Atmos Oceanic Tech 30:2168–2188

Janssen PA (1991) Quasi-linear theory of wind wave generation applied to wave forecasting. J Phys Oceanogr 21:1631–1642

Janssen P A (2004) Interactions of ocean waves and wind. Cambrige Univ. Press, 300 pp

Jenkins AD (1992) Quasi-linear eddy-viscosity model for the flux of energy and momentum to wind waves using conservation law equations in a curvilinear coordinate system. J Phys Oceanogr 22: 843–858

Kawai S (1981) Visualisation of air flow separation over wind wave crest under moderate wind. Bound-Layer Meteorol 21:93–104

Kawai S (1982) Structure of air flow separation over wind wave crest. Bound-Layer Meteorol 23:503–521

Kawamura H, Toba Y (1988) Ordered motion in turbulent boundary layer over wind waves. J Fluid Mech 197:105–138

Makin VK, Kudryavtsev VN, Mastenbroek C (1995) Drag of the sea surface. Bound-Layer Meteorol 73:159–182

Miles JW (1957) On the generation of surface waves by shear flow. Part I. J Fluid Mech 3:185–204

Moin P, Kim J (1985) The structure of the vorticity field in the turbulent channel flow. Part 1. Analysis of instantaneous fields and statistical correlations. J Fluid Mech 155:441–464

Powell MD, Vickery PJ, Reinhold TA (2003) Reduced drag coefficient for high wind speeds in tropical cyclones. Nature 422:279–283

Reul N, Branger H, Giovanangeli J-P (1999) Air flow separation over unsteady breaking waves. Phys Fluids 11(7):1959–1961

Reul N, Branger H, Giovanangeli J-P (2008) Air flow structure over short-gravity breaking water waves. Bound-Layer Meteorol 126: 477–505

Reutov VP, Troitskaya YI (1995) On nonlinear effects due to water wave interaction with turbulent wind. Izv Russ Acad Sci Atmos Ocean Phys 31:825–834

Smolyakov AV (1973) Spectrum of the quadruple radiation of the plane turbulent boundary layer. Acoust Phys 19(3):420–425

Sullivan PP, McWilliams JC, Moeng C-H (2000) Simulation of turbulent flow over idealized water waves. J Fluid Mech 404:47–85

Troitskaya YI, Rybushkina GV (2008) Quasi-linear model of interaction of surface waves with strong and hurricane winds. Izv Atmos Ocean Phys 44(4):621–645

Troitskaya YI, Sergeev D, Ermakova O, Balandina G (2011) Statistical parameters of the air turbulent boundary layer over steep water waves measured by the PIV technique. J Phys Oceanogr 41:1421–1454

Troitskaya YI, Ezhova EV, Sergeev DA, Kandaurov AA, Baidakov GA, Vdovin MA, Zilitinkevich SS (2013) Momentum and buoyancy exchange in a turbulent air boundary layer over a wavy water surface. Part 2. Wind wave spectra. Nonlinear Process Geophys 20:841–856

Veron F, Saxena G, Misra SK (2007) Measurements of the viscous tangential stress in the airflow above wind waves. Geophys Res Lett 34, L19603. doi:10.1029/2007GL031242

Vickery VJ, Wadhera D, Powell MD, Chen Y (2009) A hurricane boundary layer and wind field model for use in engineering applications. J Appl Meteorol Climatol 48:381–405